university of groningen

University Medical Center Groningen

University of Groningen

A thermo-mechanical study of mode I, small-scale yielding crack-tip fields in glassy polymers

Basu, S.; van der Giessen, E.

Published in:
International Journal of Plasticity

DOI:
10.1016/S0749-6419(02)00009-8

IMPORTANT NOTE: You are advised to consult the publisher's version (publisher's PDF) if you wish to cite from it. Please check the document version below.

Document Version
Publisher's PDF, also known as Version of record

Publication date:
2002

Link to publication in University of Groningen/UMCG research database

Citation for published version (APA):
Basu, S., & van der Giessen, E. (2002). A thermo-mechanical study of mode I, small-scale yielding crack-tip fields in glassy polymers. *International Journal of Plasticity*, *18*(10), 1395 - 1423. [PII S0749-6419(02)0009-8]. https://doi.org/10.1016/S0749-6419(02)00009-8

Copyright
Other than for strictly personal use, it is not permitted to download or to forward/distribute the text or part of it without the consent of the author(s) and/or copyright holder(s), unless the work is under an open content license (like Creative Commons).

The publication may also be distributed here under the terms of Article 25fa of the Dutch Copyright Act, indicated by the “Taverne” license. More information can be found on the University of Groningen website: https://www.rug.nl/library/open-access/self-archiving-pure/taverne-amendment.

Take-down policy
If you believe that this document breaches copyright please contact us providing details, and we will remove access to the work immediately and investigate your claim.

Downloaded from the University of Groningen/UMCG research database (Pure): http://www.rug.nl/research/portal. For technical reasons the number of authors shown on this cover page is limited to 10 maximum.

Download date: 05-05-2023

PERGAMON

International Journal of Plasticity 18 (2002) 1395–1423

INTERNATIONAL JOURNAL OF Plasticity

www.elsevier.com/locate/ijplas

A thermo-mechanical study of mode I, small-scale yielding crack-tip fields in glassy polymers

Sumit Basu*, Erik Van der Giessen

University of Groningen, Department of Applied Physics, Nijenborgh 4, 9747 AG Groningen, The Netherlands

Received in final revised form 15 September 2001

Abstract

The objective of this work is to study the stress and temperature fields ahead of a blunted notch under mode I, small-scale yielding situations. The investigation is motivated by the observation that certain polymers and polymer blends exhibit a marked increase in fracture toughness with increase in loading rate. To this end, the thermo-mechanics of glassy polymers within the framework of finite deformation elasto-viscoplasticity is discussed along with a finite element procedure to solve the resulting coupled equations. The results indicate that heat diffusion from the plastic zone leads to wider shear bands and larger heat-affected zones. Moreover, increase in loading rate has a noticeable effect on the rate of temperature rise, crack-tip opening displacement and the stress intensity factor at which crazing is expected to initiate in front of the crack tip. © 2002 Elsevier Science Ltd. All rights reserved.

Keywords: Fracture toughness; Stress intensity factor; Thermomechanical processes; Constitutive behaviour; Polymeric material

1. Introduction

The fracture toughness of polymers is known to gradually decrease with loading rate and to rise thereafter when the loading rates are further increased. In certain cases, the increase in fracture toughness with increase in loading rate is rather marked. This phenomenon has been observed in amorphous polymers, such as polystyrene (PS) and PMMA, as well as in blends based on amorphous matrix

* Corresponding author.

0749-6419/02/$ - see front matter © 2002 Elsevier Science Ltd. All rights reserved.
PII: S0749-6419(02)00009-8

polymers (Steenbrink et al., 1997). It is widely believed (e.g., Williams and Hodgkinson, 1981; Steenbrink et al., 1997) that this toughening effect is a result of heating of the material ahead of the crack tip due to plastic dissipation. This intriguing phenomenon motivates the study of the temperature fields ahead of a crack in amorphous polymers.

Early estimates of the temperature rise ahead of a running crack tip in PMMA by Williams (1972) are in the range of a few hundred degrees. Subsequent experimental observations by e.g. Döll (1976) and Fuller et al. (1975) have confirmed that these figures are reasonable. Recently, Dickinson et al. (1994) have made measurements of the amount of heat dissipated from tips of growing cracks in polystyrene (PS), and predicted temperature rise of the order of 600 °C ahead of the tip. Micrographs of the fractured samples indicated local melting due to the high temperature rise. All these results have been obtained from studies on running cracks but indicate that considerable temperature rise is also probable ahead of stationary cracks loaded at high enough rates. Very recent dynamic experiments done by Rittel (2000) on fatigue pre-cracked specimens show temperature rise of the order of 70 °C ahead of the notch tip.

Two different sources have been suggested for the localized heating: (i) plastic work and (ii) the rupture of overstressed macromolecules (Tomashevskii et al., 1975). Ahead of a crack, the high local stress field in the plastic zone leads to plastic dissipation, which is converted to heat. The second contribution of heat production ensues when the high stresses lead to the scission of the macromolecules in the region ahead of the crack, resulting in exothermic processes. Tomashevski et al. (1975) have studied the relative importance of these two mechanisms and found that plastic dissipation is important for slow crack growth, whereas a major part of the dissipated heat is contributed by molecular scission in case of fast, brittle fracture. For instance, fast fracture of thin PET films in their experiments, led to thin zones of plasticity. Slow rupture of these films resulted in large plastic zones ahead of the crack tip and the crack growth resistance was consequently considerably higher. This indicates that plastic dissipation is larger in case of slow fracture and probably contributes significantly to the temperature rise.

Prior to crack growth, so that the second mechanism is not yet activated, the temperature field ahead of a stationary crack in a glassy polymer is the result only of dissipation in the plastic zone. In order to understand these fields in detail, two pivotal issues need consideration.

Firstly, in order to study the temperature fields in front of a crack, the mechanisms by which the work of plastic dissipation is converted into heat has to be modelled. In case of metals, the fraction of the plastic work that is converted to heat is given by the Taylor–Quinney factor (Taylor and Quinney, 1934), which has a value of about 0.9. The fraction of the work done on the specimens that is converted to heat in case of amorphous, glassy polymers, has been seen experimentally to depend somewhat on the chemical structure of the macromolecules and to range between 0.6–0.8 Rudnev et al., 1991). The rest of the energy, leading to an increase of the internal energy of the system, is, at least partially, related to the appearence of internal stresses (Godovsky, 1992).

The heat transfer mechanism in the specimen under consideration is another important issue. The heat dissipation in the specimen ranges from being adiabatic at high rates of loading to nearly isothermal at very low rates. The deformation and temperature distributions under these two extreme situations have been studied by Lai and Van der Giessen (1997) and by Van der Giessen and Lai (1999), respectively. A more general approach is to allow heat conduction to take place in the material and to investigate regimes of loading rates where thermal conductivity could play a role in determining the crack tip fields.

The objective of this paper is to present such coupled thermo-mechanical studies of a stationary crack in a glassy polymer, under mode I small-scale yielding conditions. The relevance of the results is two-fold. The first is to determine the regimes of loading rates where either isothermal or adiabatic calculations hold. The second objective is to see how, in the intermediate regime, where coupled calculations are warranted, thermal conductivity of the material alters the nature of the crack tip fields.

The paper is organized in the following manner. Section 2 deals with the formulation of the set of coupled governing equations. This requires due consideration of the constitutive equations in order to determine the dissipation rate. The constitutive models that have been used are of the type proposed by Boyce et al. (1988) and modified Wu and Van der Giessen (1993), which take into account the appearance of internal stresses arising from the deformation-induced change of the molecular orientation. Section 3 briefly reviews the numerical scheme employed in this study. Results are presented in Section 4, assuming properties of styrene-acrylonitrile (SAN), which is a typical amorphous polymer but still can sustain relatively large plastic strains.

2. Governing equations

The key ingredients in the calculations are the viscoplastic constitutive model for glassy polymers and the heat flow equation that couples the energy dissipation during plastic flow to the local temperature rise. The constitutive model is similar to that proposed first by Boyce et al. (1988), but in the form discussed by Wu and Van der Giessen (1993). Coupled thermomechanical analyses have been carried out by Arruda et al. (1995), and we will be using essentially the same procedure. However, there are specific aspects of the constitutive model, related to the configurational entropy of the molecular network, that has created some confusion (see e.g. Buckley and Jones, 1995). For this reason, this section sets out to carefully analyse the thermodynamics consequences of these aspects in order to give a sound foundation to the final governing equations.

2.1. Constitutive assumptions

As discussed in more detail by Boyce et al. (1988) and Van der Giessen (1997), the large strain plastic response of glassy polymers involves: (i) rate and temperature-

dependent yield; (ii) strain softening immediately after yield; (iii) anisotropic re-hardening upon continued straining. The first two of these will be discussed later in Section 2.5. Strain hardening originates from the stretching of the network-like molecular structure during plastic flow. This network is usually regarded to be due to physical entanglements of the long molecular chains. Thus, it bears a definite resemblance to the network structure of rubbers even though the nodes are formed then by chemical cross-links. The network in rubbers endows the material with elastic stiffness through the reduction of the entropy in the molecular chains as they are stretched (see Treloar, 1975). The similarity with rubber elasticity has been used by several authors, dating back to Haward and Thackray (1968), and including Boyce et al. (1988) and Wu and Van der Giessen (1993), to formulate a constitutive law for the strain hardening in glassy polymers. However, there is a very important distinction that merits a deeper consideration of the physics.

Rubber elasticity is basically a kinetic theory, much like that of a gas (Treloar, 1975). The long-chain molecules consists of stiff chains with rather freely rotating links. Because of the weak secondary forces between molecules, the thermal energy of atoms of a long-chain molecule implies much larger amplitudes perpendicular to the chain than in the chain direction. The associated entropy is proportional to the number of configurations available in the chain. While the thermal energy in a gas is directly related to the pressure, the orientation dependence of thermal vibrations in long-chain molecules leads to longitudinal tension. Stretching of a rubber material means stretching of the chains, which occurs by rotation of the links and alignment with the stretching direction. This changes the orientation dependence of the thermal vibrations to the extent that the entropy tends to reduce. Thus, the notion of rubber elasticity based on the entropy of the configurations of the molecules. A non-Gaussian statistical treatment of a chain with N segments leads to the relation between the configurational entropy s_c and the stretch λ, and upon neglecting the internal energy changes during stretching, the free energy of a single chain is $f_c = -s_c(\lambda)T$ with

$$s_c(\lambda) = -kN\left(\frac{\lambda}{\sqrt{N}}\beta + 1n\frac{\beta}{\sinh\beta}\right), \beta = \mathcal{L}^{-1}\left(\frac{\lambda}{\sqrt{N}}\right). \tag{1}$$

Here, k is Boltzmann's constant and $\mathcal{L}^{-1}$. is the inverse of the Langevin function, $\mathcal{L}(\beta) = \coth\beta - 1/\beta$. When the contributions of individual chains are averaged over the network (see also Wu and Van der Giessen, 1993), the free energy of a rubber, f, subjected to principal strains λ_i can be expressed as

$$f(\lambda_i, T) = -C^R\int_0^{\pi}\int_0^{2\pi} N\left(\frac{\lambda}{\sqrt{N}}\beta + 1n\frac{\beta}{\sinh\beta}\right)\mathcal{C}(\theta, \phi; \lambda)\sin\theta d\theta d\phi \tag{2}$$

where $\mathcal{C}$ is the orientation distribution function of the molecular chains. The rubber modulus $C^R = nkT$ depends on the number of molecular chains per unit volume, n and is linear in temperature, a direct imprint of the entropic nature of rubber elasticity.

The accommodation by neighboring material of the rotations of links in the molecular chains requires a sufficiently high mobility. In rubbers, this is provided by the average thermal energy. In the glassy state, however, the mobility of the network is so much reduced that the molecular network is 'frozen in'. Additional energy needs to be supplied through work to enable segment rotation; this is the origin of yield in glassy polymers. Once yield takes place, the molecular network can be stretched and this gives rise to strain hardening. As the network is stretched, one can still characterize the randomness of the configuration in terms of configurational entropy, but this is no longer correlated to the thermal energy as it was in rubbers. Therefore, this kind of entropy plays a distinctly different role in the thermodynamics of a glassy polymer than in a rubber. Associated with this, the network stretching in rubbers is reversible, but in glassy polymers it is not: the associated free energy is locked in the glassy material. Nevertheless, one can borrow the description of the rubber elastic free energy and use that to describe strain hardening in glassy polymers, as long as one is carefully aware of the conceptual differences.

2.2. Thermodynamics

The above ideas will now be further elaborated by interpreting the response of a glassy polymer within the framework of the natural reference state (Besseling and Van der Giessen, 1994) or the closely related concept of the intermediate reference state. It is the state that a material point attains when its stress (Cauchy stress $\boldsymbol{\sigma}$) is reduced to zero and the temperature T to a reference temperature T_0, i.e., equal to the stress and temperature in the undeformed reference configuration. This process from the current state to the natural reference state is thermoelastic, i.e. fully reversible. Plastic deformation and the internal processes associated with this, such as strain softening and orientational hardening, are processes that change the configuration in the natural reference state. But in between the natural reference state and the current state these remain frozen. The free energy of the material point in the natural reference state does not need to vanish; only the reversible thermoelastic energy f_e (per unit mass) does. The free energy in the natural reference state, f_p (per unit mass), represents energy that is frozen into the material as a consequence of the plastic, irreversible processes. The total free energy therefore is

$$f = f_e + f_p, \tag{3}$$

but only the elastic part f_e is a thermodynamic state function. The plastic part is not a state function, but in fact just the accumulated value of $\dot{f}_p$ over time.

We will postpone the interpretation of $\dot{f}_p$ for glassy polymers until after consideration of the reversible, thermoelastic processes. For this purpose, we start off from the following expression that is routinely obtained (see, Besseling and Van der Giessen, 1994) from the local energy balance and the balance of entropy:

$$T\rho\dot{\eta} = \boldsymbol{\sigma} : \boldsymbol{D} - \rho\left(\dot{f} + \dot{T}s\right) = \frac{\boldsymbol{q}}{T}\cdot\nabla T. \tag{4}$$

Here, $\dot{\eta}$ is the entropy production rate in the entropy balance,

$$\rho\dot{s} = -\nabla\cdot(\boldsymbol{q}/T) + \rho\dot{\eta}, \tag{5}$$

which has to be nonnegative according to the Second Law of thermodynamics, $\boldsymbol{D}$ is the stretching tensor, f the specific free energy, $\boldsymbol{q}$ the heat flux vector and ∇ the vector del operator. The general expression (4) is to be supplemented with physical content by means of selection of the state variables that describe the reversible processes. The above discussion of the natural reference state immediately points to the elastic free energy, the stress $\boldsymbol{\sigma}$, the temperature T and the elastic Lagrangean-type strain tensor $\boldsymbol{E}_{\mathrm{e}}$ defined by

$$\boldsymbol{E}_{\mathrm{e}} = \frac{1}{2}\left(\boldsymbol{F}_{\mathrm{e}}^{T}\cdot\boldsymbol{F}_{\mathrm{e}} - \boldsymbol{I}\right) \tag{6}$$

with $\boldsymbol{F}_{\mathrm{e}}$ the deformation gradient from reference to current configuration. Making the (common) assumption that the elastic free energy is a function of T and $\boldsymbol{E}_{\mathrm{e}}$, $f_{\mathrm{e}}=f_{\mathrm{e}}(T, \boldsymbol{E}_{\mathrm{e}})$, substitution of (3) into (4) leads to

$$T\rho\dot{\eta} = \left(\boldsymbol{F}_{\mathrm{e}}^{-1}\cdot\boldsymbol{\sigma}\cdot\boldsymbol{F}_{\mathrm{e}}^{-1} - \rho\frac{\partial f_{\mathrm{e}}}{\partial \boldsymbol{E}_{\mathrm{e}}}\right) : \dot{\boldsymbol{E}}_{\mathrm{e}} - \rho\left(\frac{\partial f_{\mathrm{e}}}{\partial T} + s\right)\dot{T} + \boldsymbol{\sigma} : \boldsymbol{D}_{\mathrm{p}} - \rho\dot{f}_{\mathrm{p}} - \frac{\boldsymbol{q}}{T}\cdot\nabla T \tag{7}$$

after some manipulations. The first two terms on the right-hand side are associated with (reversible) changes of the independent state variables $\boldsymbol{E}_{\mathrm{e}}$ and T respectively; the remaining terms involve irreversible changes. A standard procedure in thermodynamics, based on the fact that reversible changes produce no entropy, then leads to the state equations

$$\boldsymbol{\sigma} = \rho\boldsymbol{F}_{\mathrm{e}}\cdot\frac{\partial f_{\mathrm{e}}}{\partial \boldsymbol{E}_{\mathrm{c}}}\cdot\boldsymbol{F}_{\mathrm{e}}^{\mathrm{T}}, \tag{8a}$$

$$s = -\frac{\partial f_{\mathrm{e}}}{\partial T}, \tag{8b}$$

and leaves the condition

$$T\rho\dot{\eta} = \boldsymbol{\sigma} : \boldsymbol{D}_{\mathrm{p}} - \rho\dot{f}_{\mathrm{p}} - \frac{\boldsymbol{q}}{T}\cdot\nabla T \geqslant 0 \tag{9}$$

to be satisfied by the irreversible processes. It is important to notice now that the state Eq. (8b) relates entropy only to the thermoelastic free energy and not to the plastic energy. When it is assumed that heat conduction is isotropic and governed by

$$\boldsymbol{q} = -k\nabla T, k > 0 \tag{10}$$

the last term in (9) is positive. This leaves only the condition that the plastic dissipation

$$T\rho\dot{\eta}_{\mathrm{p}} \equiv \boldsymbol{\sigma} : \boldsymbol{D}_{\mathrm{p}} - \rho\dot{f}_{\mathrm{p}} \tag{11}$$

must be nonnegative. Note that this expresses the fact that part of the plastic work (per unit time), $\boldsymbol{\sigma}$: $\boldsymbol{D}_{\mathrm{p}}$, is stored as plastic energy f_{p} and that only the remainder is dissipated. Substitution of (10) into (9) and elimination of the entropy production in (5) leads to the following expression for the rate of change of the entropy

$$T\rho\dot{s} = \left(\boldsymbol{\sigma} : \boldsymbol{D}_{\mathrm{p}} - \rho\dot{f}_{\mathrm{p}}\right) + k\nabla\cdot\nabla T \tag{12}$$

2.3. Equations of state

Assuming isotropic thermoelasticity and limiting attention to small elastic strains, $\boldsymbol{F}_{\mathrm{e}} \approx \boldsymbol{R}_{\mathrm{e}}(\boldsymbol{I} + \boldsymbol{E}_{\mathrm{e}})$, and small deviations from the reference temperature T_0, we take f_{e} in the usual form

$$\rho f_{\mathrm{e}} = -\frac{\rho c_{\mathrm{v}}}{2T_0}(T - T_0)^2 - C\alpha_{\mathrm{c}}(T - T_0)I_1 + \frac{1}{2}CI_1^2 + 2GI_2, \tag{13}$$

with the invariants $I_1 = \mathrm{tr}\boldsymbol{E}_{\mathrm{e}}$ and $I_2 = \mathrm{tr}\boldsymbol{E}'^2_{\mathrm{e}}$,$\boldsymbol{E}'_{\mathrm{e}}$ being the deviator of $\boldsymbol{E}_{\mathrm{e}}$. Application of (8) yields

$$s = c_{\mathrm{v}}\frac{T - T_0}{T_0} + \frac{C\alpha_{\mathrm{c}}}{\rho}I_1, \tag{14}$$

$$\boldsymbol{\sigma} = C[I_1 - \alpha_{\mathrm{c}}(T - T_0)]\boldsymbol{I} + 2G\boldsymbol{R}_{\mathrm{e}}^{\mathrm{T}}\cdot\boldsymbol{E}'_{\mathrm{e}}\cdot\boldsymbol{R}_{\mathrm{e}}. \tag{15}$$

The four material constants are: the bulk and shear moduli C and G, the cubic thermal expansion coefficient α_{c} and the specific heat c_{v} (at constant volume $I_1 = 0$; the specific heat at constant pressure simply derives as $c_{\mathrm{p}} = c_{\mathrm{v}} + C\alpha_{\mathrm{c}}^2 T_0/\rho$).

Straightforward time differentiation of (14) and (15) leads to the rate equations

$$\dot{s} = c_{\mathrm{v}}\frac{\dot{T}}{T_0} + \frac{C\alpha_{\mathrm{c}}}{\rho}\mathrm{tr}\boldsymbol{D}_{\mathrm{e}}, \tag{16}$$

$$\overset{\nabla}{\boldsymbol{\sigma}} = \mathcal{L}^{\mathrm{e}} : \boldsymbol{D}_{\mathrm{e}} - C\alpha_{\mathrm{c}}\dot{T}\boldsymbol{I}. \tag{17}$$

with $\overset{\nabla}{\boldsymbol{\sigma}} = \dot{\boldsymbol{\sigma}} - \boldsymbol{W}\boldsymbol{\sigma} + \boldsymbol{\sigma}\boldsymbol{W}$ the Jaumann stress rate and the tensor of elastic moduli $\mathcal{L}^{\mathrm{e}}$ being determined by G and C in the usual way. In deriving the last expressions, we have again invoked the assumption that elastic strains are small.

2.4. Strain hardening

Considering that only the network stretching contributes to the stored, plastic free energy, we now make the actual step to borrow its constitutive equation from the

analogy with stretching of a rubber network. One may be tempted to directly take the expression (2) and to replace the stretches λ_i by their plastic parts. However, there is a source of confusion when doing this: the state function (2) is appropriate for rubbers since they are reversible; but f_p for glassy polymers refers to irreversible processes and therefore is not a point function, but evolves in time. From this point of view, it seems natural to formulate a constitutive law for f_p through an evolution equation. We therefore ask the question: how does f_p change upon a plastic strain rate $\boldsymbol{D}_p$?

When following the analogy to rubber elasticity, this leads to the question: how does the elastic energy f in a rubber change upon a strain rate $\boldsymbol{D}$? From (2), it follows that $\rho\dot{f} = \boldsymbol{b} : \boldsymbol{D}$ at constant temperature with the stress $\boldsymbol{b}$ being given by (Wu and Van der Giessen, 1995)

$$\boldsymbol{b} = C^R\sqrt{N}\int_0^{\pi}\int_0^{2\pi}\lambda\mathcal{L}^{-1}\left(\frac{\lambda}{\sqrt{N}}\right)\mathcal{C}(\theta,\phi;\lambda)\boldsymbol{m}\otimes\boldsymbol{m}\sin\theta\mathrm{d}\theta\mathrm{d}\phi - p\boldsymbol{I}, \tag{18}$$

with $\boldsymbol{m}(\theta,\phi)$ being the unit vector in orientation space. The hydrostatic pressure p arises from the common assumption that stretching of the network does not give rise to volume changes ($\mathrm{tr}\boldsymbol{D}=0$).

With this result, we can now formulate the evolution of the plastic energy associated with the networking stretching in a glassy polymer during plastic straining as

$$\rho\dot{f}_p = \boldsymbol{b} : \boldsymbol{D}_p, \tag{19}$$

with $\boldsymbol{b}$ given by the expression (18). Strictly speaking, one should replace λ in this expression with the plastic part of the stretch, but since elastic strains are assumed to be small anyway, the difference between plastic and total stretch can be neglected for all practical purposes. Substitution of (19) into (11) gives

$$T\rho\dot{\eta}_p = \overline{\boldsymbol{\sigma}} : \boldsymbol{D}_p, \quad \overline{\boldsymbol{\sigma}} = \boldsymbol{\sigma} - \boldsymbol{b} \tag{20}$$

which shows that the network stretching provides a back stress to further plastic flow. his justifies the original assumption by Haward and Thackray (1968), as used later by Boyce et al. (1988).

We note that in the computations to be presented, we do not actually calculate the back stress from (18). It has been shown by Wu and Van der Giessen (1993) that it can be accurately approximated by a nonlinear combination of the stresses according to two simplified network models:

$$\boldsymbol{b} = (1-\rho)\boldsymbol{b}^{3-ch} + \rho\boldsymbol{b}^{8-ch}. \tag{21}$$

The constitutive equations for the three-chain and eight-chain stresses $\boldsymbol{b}^{3-\mathrm{ch}}$ and $\boldsymbol{b}^{8-\mathrm{ch}}$ contain only two material parameters: the initial shear modulus C_R and N, which implies a limit stretch of $\sqrt{N}$. The weight factor $\rho = 0.85\overline{\lambda}/\sqrt{N}$ with $\overline{\lambda}$ the maximum principal plastic stretch.

It should be realized that, while n and N can be considered to be constant in rubbers, this is generally not a good assumption in glassy material where the network is formed by physical entanglements. According to Arruda et al. (1995), following studies on temperature dependent birefringence by Raha and Bowden (1972), the network density n depends on temperature according to

$$n(T) = B - D\exp(-E_a/RT) \text{ while } nN = \text{constant}, \tag{22}$$

because the numbers of molecular links remains constant. In (22), E_a is the dissociation energy, R is the universal gas constant, while B and D are material constants. As a consequence, the back stress according to (19) is a function of temperature through the dependence of N and $C^R = nkT$ on T. The material constants B and D are derived on the assumption that as $T \to T_g$, the glass transition temperature, $n(T) \to 0$. Hence, $B/D = \exp(-E_a/RT_g)$.

2.5. Viscoplastic flow

According to (20), the driving force for energy dissipation due to plastic flow is the effective stress $\overline{\boldsymbol{\sigma}} = \boldsymbol{\sigma} - \boldsymbol{b}$. The plastic strain-rate tensor $\boldsymbol{D}_p$ is then defined under the assumption that yield in amorphous polymers is an isotropic process, as follows:

$$\boldsymbol{D}_p = \frac{\dot{\gamma}_p}{\sqrt{2}\tau}\overline{\boldsymbol{\sigma}}, \quad \tau = \sqrt{\frac{1}{2}\overline{\boldsymbol{\sigma}}' : \overline{\boldsymbol{\sigma}}'}, \quad \dot{\gamma}_p = \sqrt{\boldsymbol{D}_p : \boldsymbol{D}_p}, \tag{23}$$

with $\overline{\boldsymbol{\sigma}}'$ denoting the deviatoric part of the driving stress tensor.

Yield is also intrinsically rate dependent and dependent on temperature and pressure, through the constitutive equation for $\dot{\gamma}_p$. The particular form of the function $\dot{\gamma}_p$. that is used in this work is based on Argon's (1973) model of yield in amorphous polymers, in which

$$\dot{\gamma}_p = \dot{\gamma}_0 \exp\left[-\frac{As_y}{T}\left(1 - \left(\frac{\tau}{s_y}\right)^{5/6}\right)\right], \tag{24}$$

with $s_y = s + \alpha p$ the pressure-dependent, athermal yield strength. Here, A and α are material constants. Furthermore, amorphous polymers exhibit strain softening upon yield. This is incorporated by letting s evolve with strain according to (Boyce et al., 1988)

$$\dot{s} = h(1 - s/s_{ss})\dot{\gamma}_p, \tag{25}$$

with h the initial softening modulus and s_{ss} is the ultimate minimal shear strength. It should be noted that the above constitutive model and its variants have been used for several applications (for example, see Wu and Van der Giessen, 1995a,b; Arruda et al., 1993).

2.6. Self heating

Energy dissipation leads to an increase in entropy according to (12). Using (19) and the relation (16), the resulting rate of temperature change is found to be given by

$$\rho c_{\mathrm{v}} \dot{T} = \overline{\boldsymbol{\sigma}} : \boldsymbol{D}_{\mathrm{p}} + k \nabla \cdot \nabla T. \tag{26}$$

In deriving this, contributions due to the elastic volume changes are neglected as is the difference between T_0 and T.

A few words regarding the temperature dependence of the thermal properties of polymers are in place here. Godovsky (1992) presents a review of experimental results on the variation of thermal conductivity and heat capacity of glassy polymers with temperature. In the range from room temperature to the glass transition temperature the variation in thermal conductivity and heat capacity with temperature is small for most amorphous polymers. For instance, the largest variation in thermal conductivity is manifested by PET, where k varies by about 10% in the temperature range of interest. We therefore take k to be temperature independent.

3. Computational model

Following the isothermal study of Lai and Van der Giessen (1997), the development of plasticity ahead of a blunted crack tip is investigated under conditions of mode I loading. Attention is confined to small-scale yielding and the boundary layer approach for a stationary plane strain crack is adopted. The model problem studied is illustrated in Fig. 1(a). There is no heat flux through the plane ahead of the crack due to symmetry. All other boundaries are assumed to be insulated. Due to mode I symmetry, only half of the problem needs to be analyzed. Fig. 1(b) shows the finite element mesh used. The mesh in the region near the crack tip is shown in Fig. 1(c). The same mesh is used to analyze both the mechanical and the thermal problems. Along the remote boundary, the elastic displacement rates are prescribed in accordance with the chosen rate of change of the applied stress intensity factor K_{I}.

A series of isothermal, adiabatic and coupled analyses are conducted at different loading rates. The isothermal cases represent very slow processes where sufficient time is allowed for the system to be at thermal equilibrium with the surroundings, i.e. $\dot{T} = 0$ everywhere. On the contrary, adiabatic cases represent very fast processes, where the heat essentially does not get enough time to diffuse. The second term on the right hand side of (26) becomes negligible in comparison to the first.

The computational model involves the coupled solution of the equilibrium conditions, the constitutive Eqs. (17) and the thermal Eq. (26). An incremental approach is used, adopting the rate tangent modulus method due to Pierce et al. (1984). In this method the effective plastic shear strain rate $\dot{\gamma}_{\mathrm{p}}$ within an increment is expressed as a linear combination of its values at times t and $t + \Delta t$ by

$$\dot{\gamma}_{\mathrm{p}} = (1 - \theta)\dot{\gamma}_{\mathrm{p}}(t) + \theta \dot{\gamma}_{\mathrm{p}}(t + \Delta t), \tag{27}$$

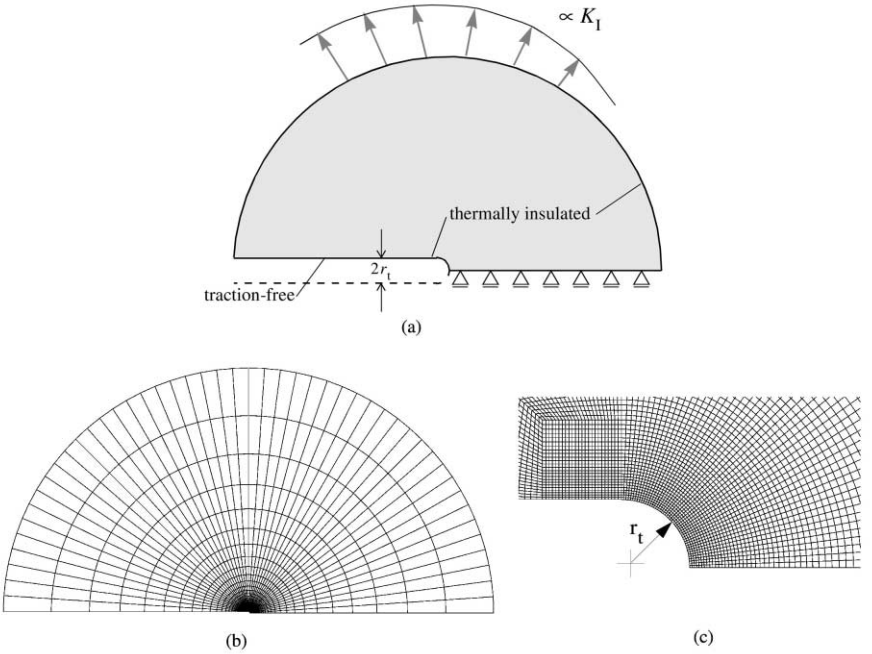

Fig. 1. (a) Schematic of the small scale yielding problem with insulated boundaries; (b) the finite element mesh used in the analyses and (c) the near-tip mesh.

where θ is a parameter ranging from zero to unity. The plastic strain rate at time $t + \Delta t$ is approximated by

$$\dot{\gamma}_{\mathrm{p}}(t + \Delta t) = \dot{\gamma}_{\mathrm{p}}(t) + \theta \Delta t \frac{\partial \dot{\gamma}_{\mathrm{p}}}{\partial \tau} \dot{\tau} + \theta \Delta t \frac{\partial \dot{\gamma}_{\mathrm{p}}}{\partial T} \dot{T} \tag{28}$$

In addition, we use the rate form of the constitutive Eqs. (18) and (22) for the back stress tensor $\boldsymbol{b}$ in the form (see, Wu and Van der Giessen, 1996)

$$\overset{\nabla}{\boldsymbol{b}} = \mathcal{R} : \boldsymbol{D}. \tag{29}$$

Using the above equations, the Jaumann rate of the Cauchy stress tensor is ultimately expressed as

$$\overset{\nabla}{\boldsymbol{\sigma}} = \mathcal{L} : \boldsymbol{D} + \dot{\boldsymbol{\sigma}}_{\mathrm{v}} + \dot{\boldsymbol{\sigma}}_{\mathrm{T}}. \tag{30}$$

The terms defining the rate tangent modulus tensor $\mathcal{L}$ are given in Table 1.

The governing equations are solved using a Total Lagrangian approach in terms of the second Piola–Kirchoff stress tensor and the work conjugate Lagrangian strain (details may be found in Wu and Van der Giessen, 1996). We note that the vector del operator ∇ in (26) is related to the corresponding operator in the undeformed

Table 1
Terms defining the rate tangent modulus tensor $\mathcal{L}$ in (30)

$$\mathcal{L} = \mathcal{L}^{e} - \lambda \boldsymbol{M} \otimes \boldsymbol{M}$$

$$\dot{\boldsymbol{\sigma}}_{v} = \frac{\dot{\gamma}_{p}}{1+\zeta}\boldsymbol{M}, \quad \dot{\sigma}_{T} = \left(\sqrt{2}\lambda \frac{\partial \dot{\gamma}_{p}/\partial T}{\partial \dot{\gamma}_{p}/\partial \tau} + C\alpha_{c}\boldsymbol{I}\right)\dot{T}\boldsymbol{M},$$

$$\boldsymbol{M} = \frac{2G}{\sqrt{2}\tau}\overline{\boldsymbol{\sigma}}', \quad \lambda = \frac{1}{\sqrt{2}}\frac{\zeta}{g(1+\zeta)}.$$

$$g = \frac{1}{\sqrt{2}}\left[2G + \frac{1}{2\tau^{2}}\boldsymbol{\sigma}' : \mathcal{R}' : \boldsymbol{\sigma}'\right], \quad \zeta = g\theta\Delta t\frac{\partial \dot{\gamma}_{p}}{\partial \tau}.$$

configuration, ∇_0, according to $\nabla_0 = \boldsymbol{F}^{T}\cdot\nabla$. The diffusion term in (26) thus transforms as

$$\nabla\cdot\nabla = \nabla_0\cdot\left(\boldsymbol{F}^{-1}\cdot\boldsymbol{F}^{-T}\right)\cdot\nabla_0. \tag{31}$$

This agrees with the formulation of Zhou et al. (1994).

The differential equations resulting from the finite element discretization of the variational equations associated with the momentum and the energy balance equations are of the form:

$$\boldsymbol{K}\dot{\boldsymbol{U}} = \dot{\boldsymbol{F}}_{t} + \dot{\boldsymbol{\chi}}_{v} + \dot{\boldsymbol{\chi}}_{T}, \tag{32}$$

$$\boldsymbol{C}\dot{\Theta} + \boldsymbol{D}\Theta = \mathcal{D}, \tag{33}$$

where $\boldsymbol{U}$ and Θ are the vectors of nodal displacements and temperatures. The vectors $\dot{\boldsymbol{\chi}}_{v}$ and $\dot{\boldsymbol{\chi}}_{T}$ arise due to viscoplasticity and thermal sensitivity [cf. $\dot{\boldsymbol{\sigma}}_{v}$ and $\dot{\boldsymbol{\sigma}}_{T}$ in (30)] respectively, while $\mathcal{D}$ is the heat source vector due to plastic dissipation. The Eq. (33) is integrated in time by the central difference scheme. In this method, the temperature $\Theta^{t+\Delta t}$ is approximated in terms of Θ^{t} as

$$\Theta^{t+\Delta t} = \Theta^{t} + \left[(1-\beta)\dot{\Theta}^{t} + \beta\dot{\Theta}^{t+\Delta t}\right]\Delta t, \tag{34}$$

which results in an unconditionally stable algorithm for $\beta \geqslant 0.5$.

The system of coupled Eqs. (32)–(33) is solved in a staggered manner with very small time steps. The time step size is decided based on the algorithm proposed by Van der Giessen and Neale (1993). Supposing the solution at time t is known, we use the rate tangent modulus method to obtain a solution to (32) at time $t+\Delta t$. The solution to (32) yields the dissipation vector $\mathcal{D}$, which is then used to compute $\Theta^{t+\Delta t}$. When the time step size is very small, this staggered scheme produces satisfactory results.

The material properties chosen for the specimen are relevant for SAN (Steenbrink et al., 1997) and read: $G = 543.5$ MPa, $\upsilon = 0.38$, $s_0 = 120$ MPa, $A = 129$ K/MPa, $\dot{\gamma}_0 = 1.06\times10^{8}$ s^{-1}, $\alpha = 0.25$, $h = 1500$ MPa, and $s_{ss} = 95$ MPa. The hardening parameters at room temperature (296 K) are taken to be $C_R = 4$MPa and $N = 12$, while

the dissociation energy is estimated as $E_a/R = 2.8\times10^3$ K. The cubic thermal expansion coefficient α_c and conductivity are taken as 2×10^{-4} K^{-1} and 0.35 W/m K respectively. The glass transition temperature T_g for this material is 383 K. Finally, $\rho_0 = 1.08\times10^3$ kg/m^3 and $c_v = 1.38\times10^3$ J/kg K. The radius of the crack tip r_t is taken to be 0.1 mm}.

4. Results and discussion

4.1. Temperature-dependent plastic flow

The thermal sensitivity of polymers in this work arises from the temperature dependence of their yield stress as well as from the softening that probably results from the loosening of the entanglements with rise in temperature. While the decrease in yield stress with temperature is governed by (24), implying a linear decrease in yield stress with temperature, the dependence of entanglement density on temperature is given by (22).

In order to demonstrate the thermal sensitivity, Fig. 2 shows the difference in uniaxial stress–strain response between a specimen deformed adiabatically and isothermally, at different strain rates. The initial temperature is 296 K in all these calculations. The adiabatic and the isothermal responses of the material under this simple loading is seen to vary considerably at high strain rate. If isothermal conditions are assumed, the basic effect of an increase in strain rate is to shift the uniaxial

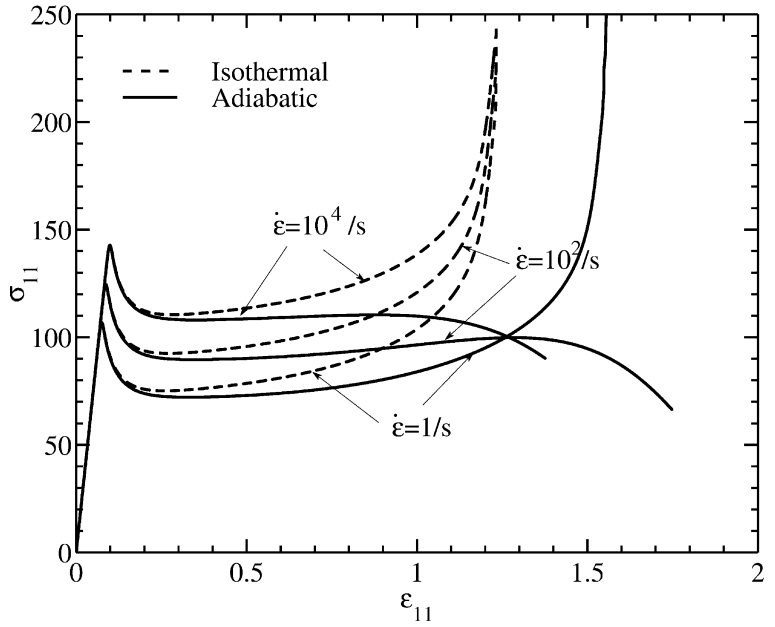

Fig. 2. Uniaxial stress–strain curves for a glassy polymer under isothermal and adiabatic conditions.

stress–strain response to a higher level without modifying the softening or hardening characteristics. However, when adiabatic conditions prevail, re-hardening can be suppressed at high enough loading rates. In fact, at strain rates above 1×10^2 s^{-1}, the material ceases to re-harden completely.

The most important origin for the difference in the adiabatic and the isothermal response under uniaxial conditions stems from the temperature dependence of the network resistance. This is illustrated in Fig. 3(a), where the ratio of the actual stretch λ to the limiting stretch $\sqrt{N}$ is plotted as a function of true strain under adiabatic conditions. It should be noted that this ratio can attain a maximum value of unity, as the material essentially locks and plastic strain rate $\dot{\gamma}_{\mathrm{p}}$ goes to zero. Additionally, in the adiabatic case, the limit stretch is a function of temperature according to (22). At low loading rates, the ratio $\lambda/\sqrt{N}$ increases monotonically with strain and quickly attains the limiting value. However, at sufficiently high loading rates, $\lambda/\sqrt{N}$ increases till a particular strain and starts to drop thereafter because of the increase of N with increasing temperature. As a consequence, the temperature in the material can rise to the glass transition temperature T_{g} without the intervention of 'locking'. This is illustrated in Fig. 3(b). All curves in this figure have been plotted up to the attainment of the limit stretch or the glass transition temperature, whichever occurred earlier. We see that the glass transition temperature is not attainable at low loading rates, because the material locks before that. However, at high loading rates, attainment of the glass transition temperature becomes possible due to effective suppression of material locking.

4.2. Rate-dependent near-tip fields

The stress and temperature fields at the tip of a crack are not only influenced by temperature-dependent plasticity as discussed above, but also through the fact that heat can leave the plastic zone by means of conduction. Isothermal and adiabatic situations can actually be conceived as special cases with infinite or zero conductivity, respectively. From a one-dimensional argument, the importance of conductivity in a particular situation can be assessed by the non-dimensional parameter κ defined as,

$$\kappa = \frac{k t_0}{\rho_0 c_{\mathrm{v}} L_0^2}, \tag{35}$$

where t_0 is a characteristic time scale and L_0 a characteristic length scale associated with the problem. For $\kappa >> 1$, isothermal calculations are expected to suffice, while for $\kappa << 1$, adiabatic condition will prevail.

If the characteristic time scale is chosen to be the time required to attain a particular value of K_{I}, then t_0 is directly related to the applied loading rate $\dot{K}_{\mathrm{I}}$ as $t_0 = K_{\mathrm{I}}/\dot{K}_{\mathrm{I}}$. In classical elastic–plastic fracture mechanics, the plane-strain plastic zone is taken to have the usual kidney shape, and the only available length scale associated with the small-scale yielding problem is the approximate size of the plastic zone

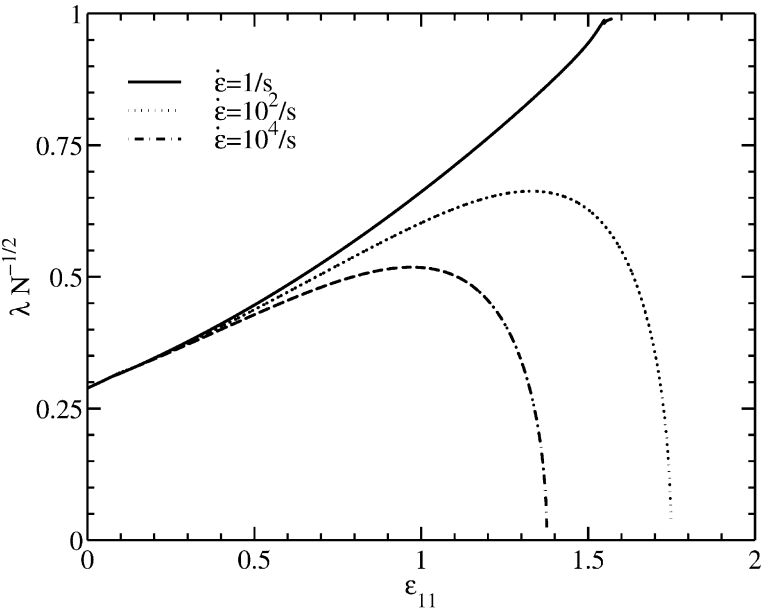

(a)

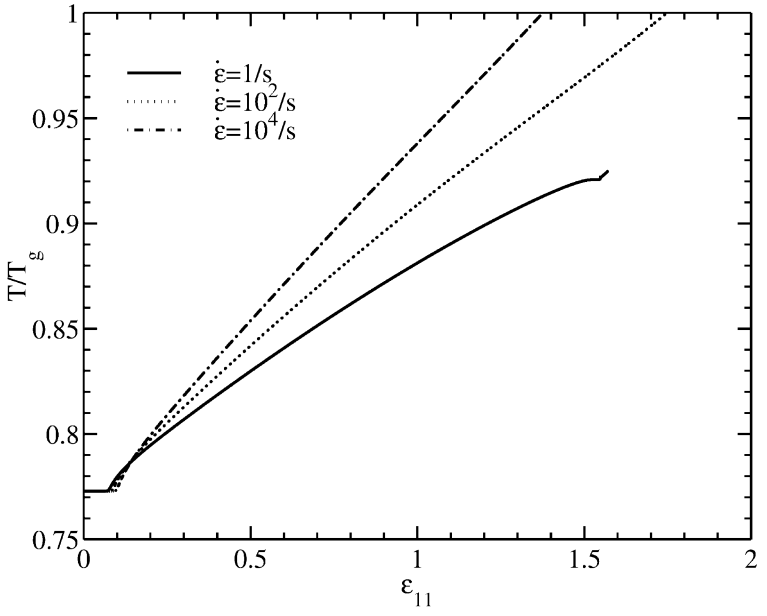

(b)

Fig. 3. Evolution of (a) the ratio of total stretch λ to the limiting stretch $\sqrt{N}$ and (b) of temperature T relative to the glass transition temperature T_g, with strain under adiabatic conditions.

$r_p \sim (K_I/s_0)^2$. Hence, under this choice of L_0, conductivity will assume importance, ie. $\kappa \simeq 1$, when

$$\dot{K}_I \simeq \frac{k s_0^4}{\rho_0 c_v K_I^3}. \tag{36}$$

For example, in order for the effect of conductivity to manifest itself at a value of $K_I \simeq 3.3$ MPa$\sqrt{\text{m}}$, the specimen has to be loaded at a $\dot{K}_I$ of the order of 10^2 MPa$\sqrt{\text{m}}$/s for the material parameters used here. Here we should add that, since there are significant differences between the plastic zone shape predicted by classical fracture mechanics and that exhibited by polymers (Lai and Van der Giessen, 1997), (36) gives only a rough estimate of the loading rate at which conductivity of the material becomes important. We will therefore explore this further using the detailed computations.

Fig. 4(a) shows the distribution of the instantaneous plastic shear rate $\dot{\gamma}_p$ at a loading rate of 1 MPa$\sqrt{\text{m}}$/s when $K_I = 3.3$ MPa$\sqrt{\text{m}}$. In this and all subsequent plots, the plastic shear rate is normalized by the parameter $\dot{\Gamma}_0$,

$$\dot{\Gamma}_0 = \frac{\dot{K}_I}{E\sqrt{2\pi r_t}} \tag{37}$$

as a reference strain rate at the tip of a notch under small-scale yielding situations (E is the Young's modulus of the material). At the load level shown in Fig. 4(a), a relatively large plastic zone has developed in front of the crack tip. As demonstrated first by Lai and Van der Giessen (1997), the plastic zone is characterized by the initiation and propagation of shear bands. At low load levels, a family of shear bands emanate from the crack tip. As the load is increased, they propagate away from the crack plane, leaving behind islands of material that has 'locked' (i.e. attained the limit stretch). At the load level shown, two main shear bands are active. The corresponding temperature rise, shown in Fig. 4(b), is seen to be very small and a nearly isothermal situation prevails at the crack tip.

Figs. 5–7 pertain to a loading rate of 10^2 MPa$\sqrt{\text{m}}$/s. According to the rough estimate made using (36), this is the rate at which the effects of conductivity should be important within a length scale comparable to the size of the plastic zone. To verify this hypothesis, two sets of analyses were done. In the first analysis, the effects of conductivity were assumed to be absent and adiabatic conditions prevail; coupled calculations were used in the other case.

Fig. 5(a) and (b) shows the contours of the plastic shear rate $\dot{\gamma}_p$ at a load level of 1.65 MPa$\sqrt{\text{m}}$ for the adiabatic and the coupled analyses, respectively. The plastic zone is rather small at this level of load and because the temperature is low, no difference between coupled and adiabatic calculations can be seen. Both Fig. 5(a) and (b) show shear bands emanating from the crack tip, which grow outward from the crack plane with increasing load and lead to the situation shown in Fig. 6(a) and (b) at a load level of 3.3 MPa$\sqrt{\text{m}}$. Although the overall features of the plastic zones seem similar for both the adiabatic and the coupled analyses, at higher levels of load the coupled analysis, Fig. 6(b), exhibits wider shear bands.

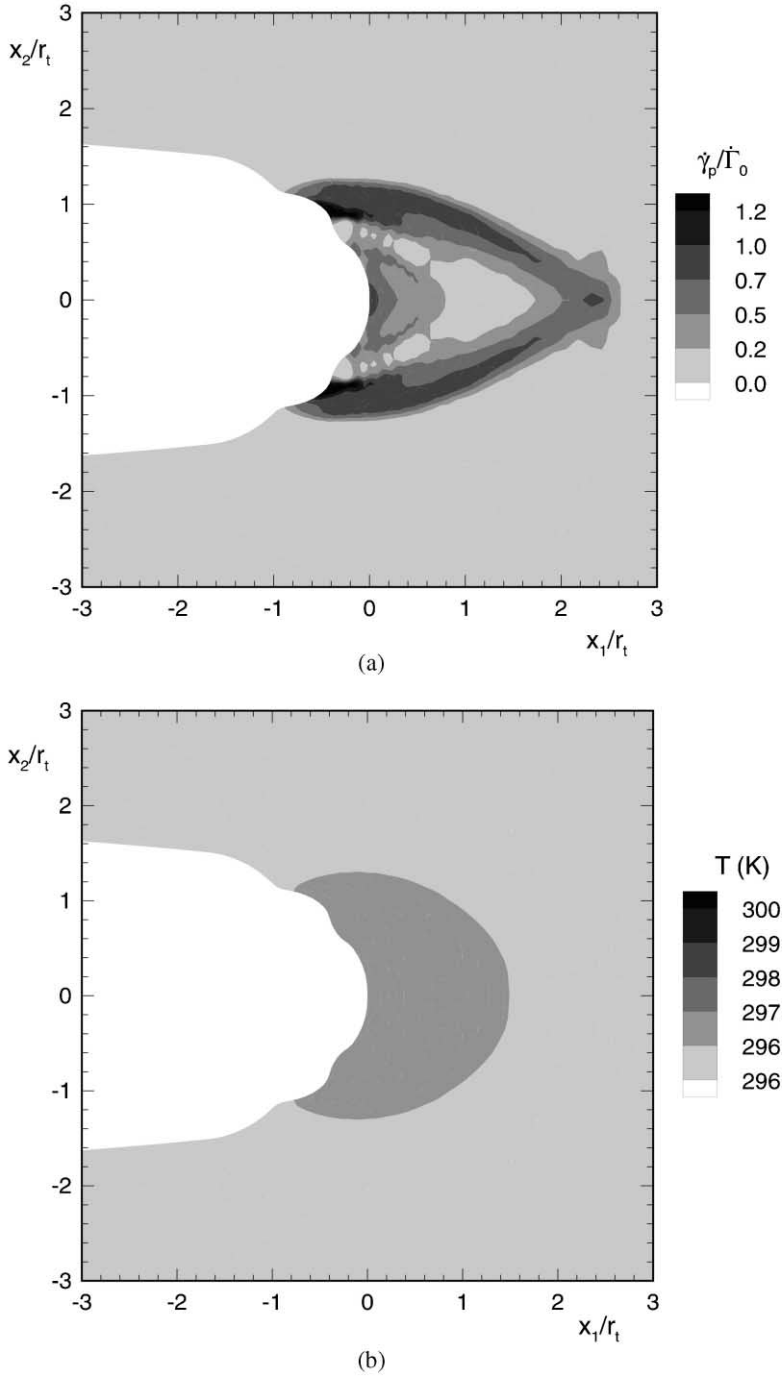

Fig. 4. Crack tip fields for a coupled analysis with $\dot{K}_I = 1$ MPa$\sqrt{\text{m}}$/s, at a load level corresponding to $K_I = 3.3$ MPa$\sqrt{\text{m}}$/s, showing the distribution of (a) plastic shear rate $\dot{\gamma}_p$ and (b) temperature.

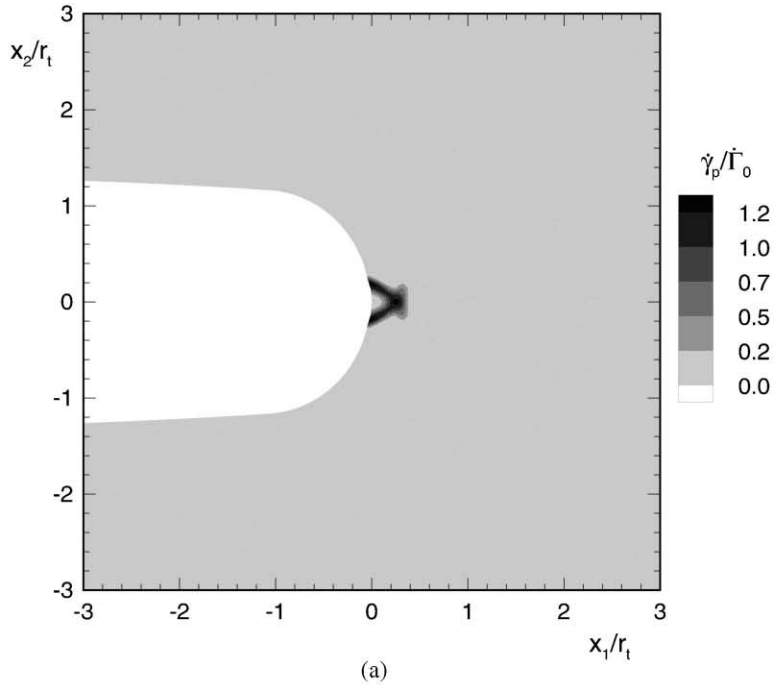

(a)

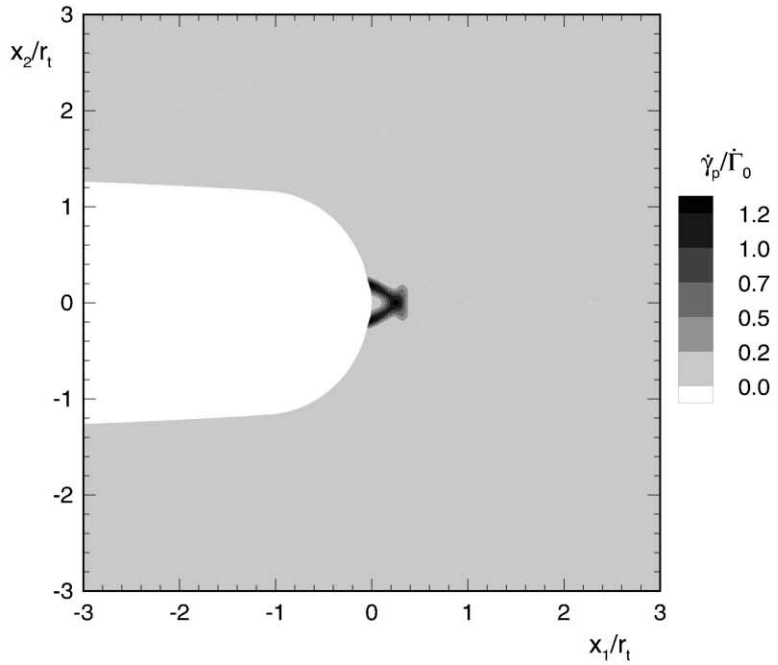

(b)

Fig. 5. Distribution of plastic shear rate $\dot{\gamma}_p$ at a crack tip for (a) an adiabatic and (b) a coupled analysis at $K_I = 1.65$ MPa$\sqrt{\text{m}}$/s and a loading rate of 10^2 MPa$\sqrt{\text{m}}$/s.

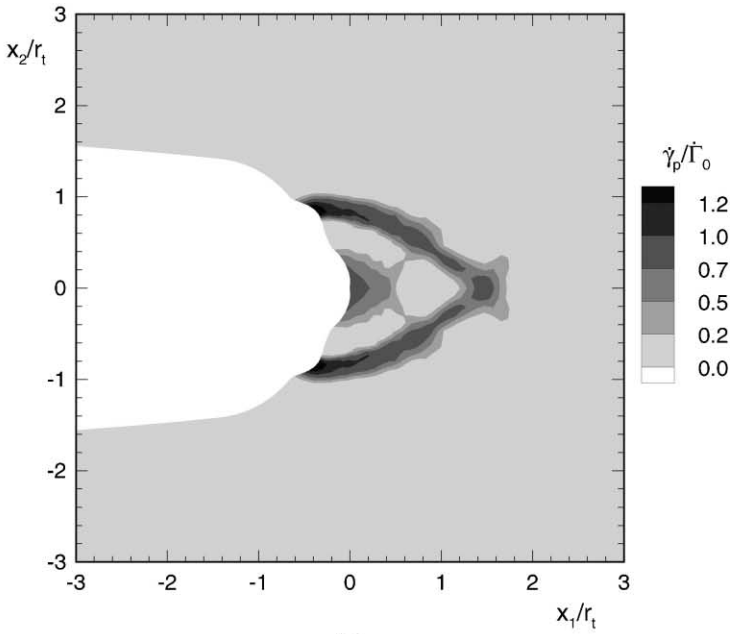

Fig. 6. Distribution of plastic shear rate $\dot{\gamma}_p$ at a crack tip for (a) an adiabatic and (b) a coupled analysis at $K_I = 3.3$ MPa$\sqrt{\text{m}}$/s and a loading rate of 10^2 MPa$\sqrt{\text{m}}$/s.

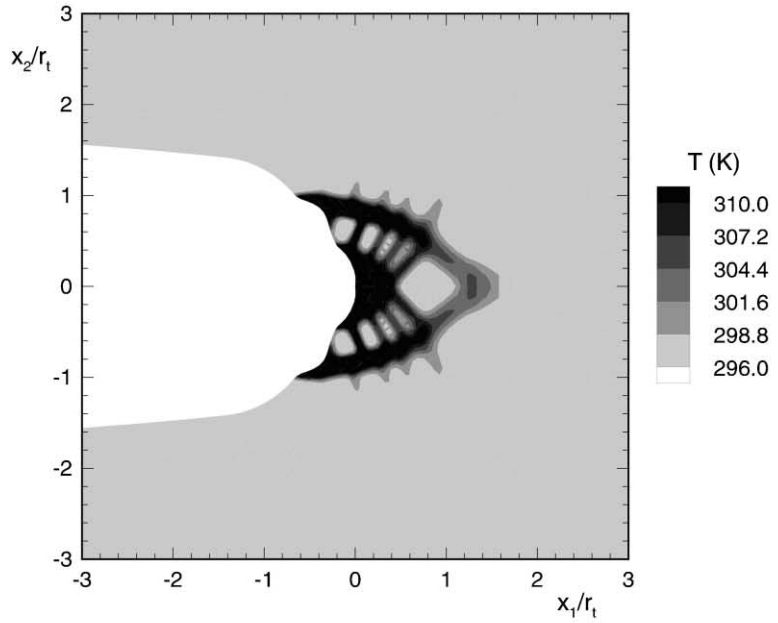

(a)

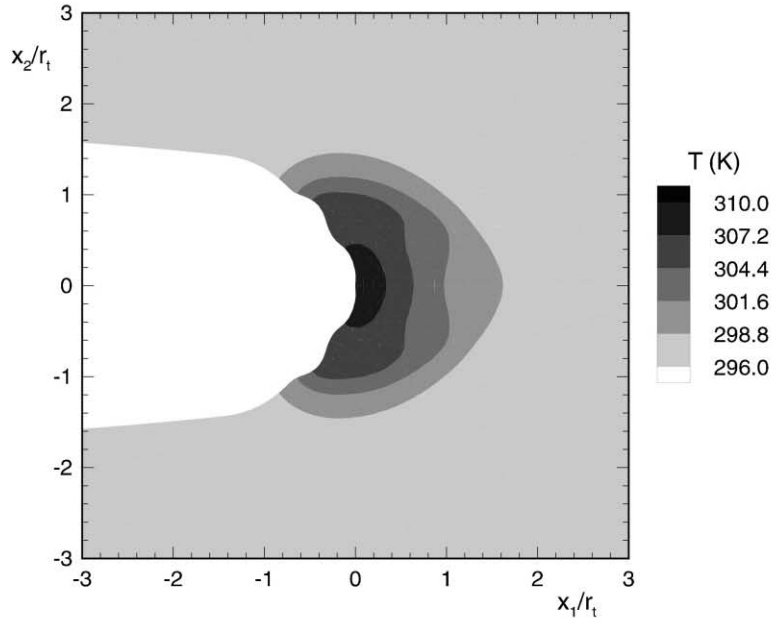

(b)

Fig. 7. Distribution of temperature at a crack tip for (a) an adiabatic and (b) a coupled analysis at $K_I = 3.3$ MPa$\sqrt{\text{m}}$/s and a loading rate of 10^2 MPa$\sqrt{\text{m}}$/s.

The reason for this is demonstrated in Fig. 7(a) and (b) where the temperature distributions for both analyses have been plotted at a load level corresponding to Fig. 6. In absence of conductivity, Fig. 7(a), the temperature distribution follows the structure of the plastic shear rate distribution. Since the stress level all over the region surrounding the crack tip is of the order of s_{ss}, high dissipation occurs at spots where the strain rates are large. As the heat cannot diffuse away from these 'hot spots' in the adiabatic analysis, these constitute the regions where the temperature level is also high. The temperature distribution becomes entirely different at this loading rate if conductivity of the material is accounted for. As shown in Fig. 7(b), the time involved in reaching a load level of 3.3 MPa$\sqrt{\text{m}}$ at the given loading rate is enough to allow the heat to affect a larger region. The heat-affected zone is not only larger but more diffuse in character, and leads to the wider shear bands as evidenced in Fig. 6(b).

An even higher loading rate of 10^4 MPa$\sqrt{\text{m}}$/s is considered in Figs. 8 and 9. Fig. 8(a) and (b) shows the temperature distribution according to the adiabatic and the coupled analyses at a load level of $K_I = 3.3$ MPa$\sqrt{\text{m}}$. It can be seen from the two figures that the temperature distribution in the coupled case is closer in appearance to the adiabatic analysis than in Fig. 7(a) and (b). Also, the temperature rise in case of the adiabatic analysis is higher than in the coupled case, so that the glass transition temperature is reached faster. The analysis in the coupled case can be continued further and the temperature distribution at a load level of 4.8 MPa$\sqrt{\text{m}}$ is shown in Fig. 9. At this level of load, enough time has been allowed for the heat to get conducted and as a result, the distribution of temperature is again quite diffuse with the initial banding almost completely smeared out.

At even higher loading rates, the deformation process tends towards the adiabatic limit, leading to small spots of high temperature and thinner shear bands. In Fig. 10, the temperature distribution along the plane ahead of the tip is shown for loading rates of 10^2 and 10^6 MPa$\sqrt{\text{m}}$/s as a function of the normalized distance $x/(K_I/s_0)^2$ ahead of the crack tip. For the higher loading rate, Fig. 10(b), a larger temperature rise is found in a zone very close to the crack tip, whereas the temperature distribution at the lower loading rate, Fig. 10(a), extends further into the material. It is noteworthy that the shape of these temperature distribution curves is qualitatively similar to those observed experimentally during fracture of PET films (Godovsky, 1992).

In order to further assess the effect of rate and thermal sensitivity, the crack opening displacement is monitored as a function of $J/(s_0 r_t)$ in Fig. 11, with $J = (1-\nu^2)\, K_I^2/E$. According to Shih (1981), based on J_2-flow theory of plasticity, with yield strength σ_0, the crack-tip opening displacement δ_t is related to the J integral as $\delta_t = d_n J/\sigma_0$, where d_n is a factor depending on the strain hardening coefficient of the material. Fig. 11, however, shows that the crack-tip opening δ_t found in the present polymer is bilinear in $J/(s_0 r_t)$. All three curves shown in the figure exhibit a distinct change at slope at some value of K_I. This change in slope indicates a slowing down of the crack opening with load and is associated with the appearance of 'locked' material at the crack tip. Moreover, as seen from the isothermal analyses at $\dot{K}_I = 1$ and 10^6 MPa$\sqrt{\text{m}}$/s, the rate of loading also leads to slowing down in the rate of crack opening with applied load. In case of the coupled

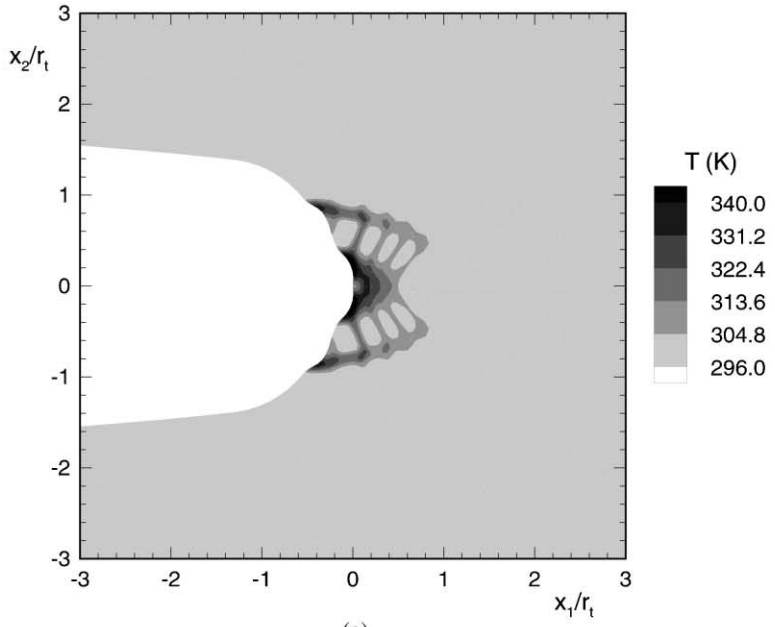

(a)

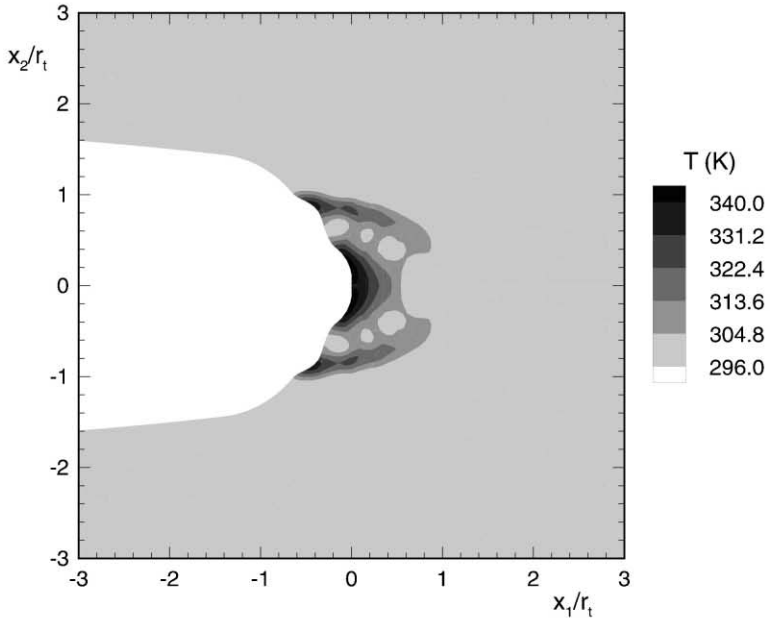

(b)

Fig. 8. Distribution of temperature at a crack tip for (a) an adiabatic and (b) a coupled analysis at $K_I = 3.3$ MPa$\sqrt{\text{m}}$/s and a loading rate of 10^4 MPa$\sqrt{\text{m}}$/s.

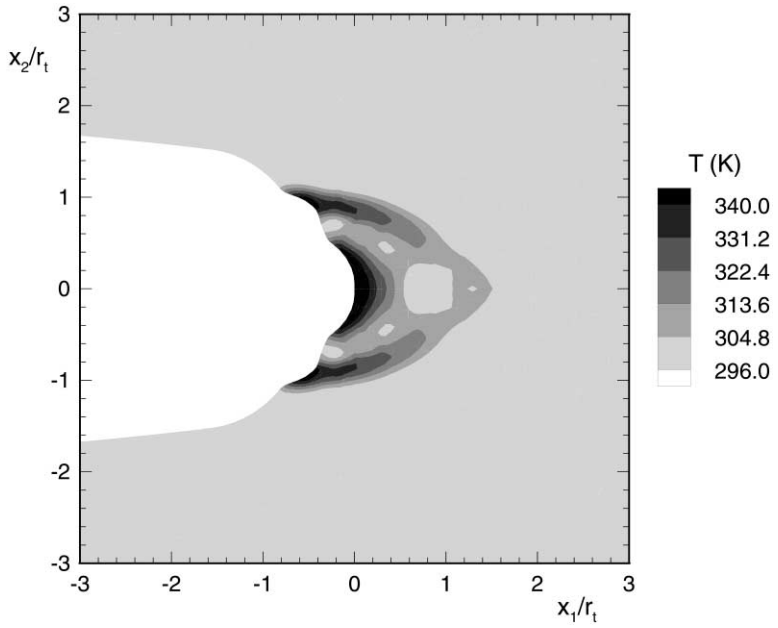

Fig. 9. Distribution of temperature at the crack tip for a coupled analysis at $K_I = 4.8$ MPa$\sqrt{\text{m}}$/s and a loading rate of 10^4 MPa$\sqrt{\text{m}}$/s.

analysis at high loading rate, where temperature rise is substantial, the crack opening rates with respect to the applied load are almost identical to those encountered in case of an isothermal analysis at the same loading rate. This means that the temperature rise of the order of 100° C caused by plastic dissipation ahead of a crack tip does not alter the material properties sufficiently to manifest itself in the crack opening displacement. It should be kept in mind that the analyses are stopped when the temperature becomes close to T_g. The effect of temperature rise on the crack opening displacement could be substantial if localised melting ahead of the tip is allowed. Heat generation can also result from exothermic chain scission in the highly stretched region ahead of the tip. This has not been considered in this analysis. Finally, it should be noted that the absence of a thermal effect on the crack opening displacement can also be different for a more thermally sensitive material (e.g. with a larger value of A).

4.3. Craze initiation

It is interesting to investigate the possible implications that the above analyses might have on the process of fracture initiation in these materials. Fracture in polymers usually occurs by 'crazing'. Crazing is a complex process, which is known to be sensitive to the mean stress ahead of a crack tip. Based on experimental work

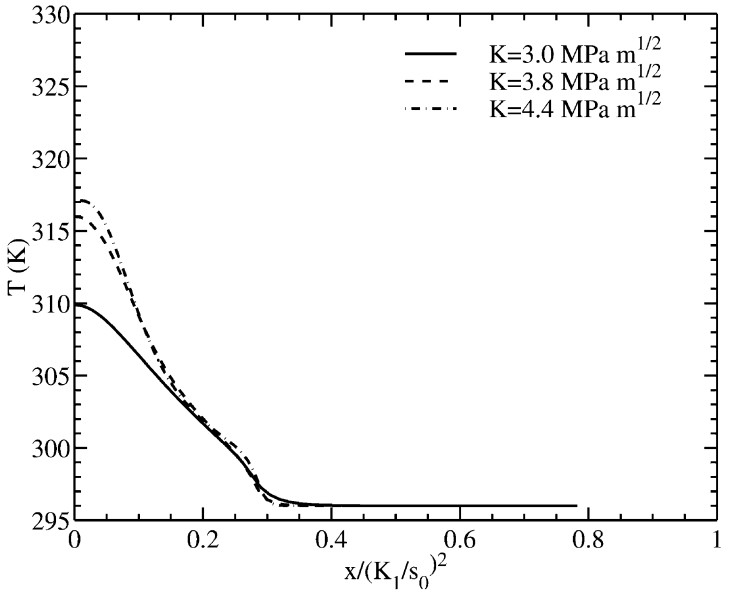

(a)

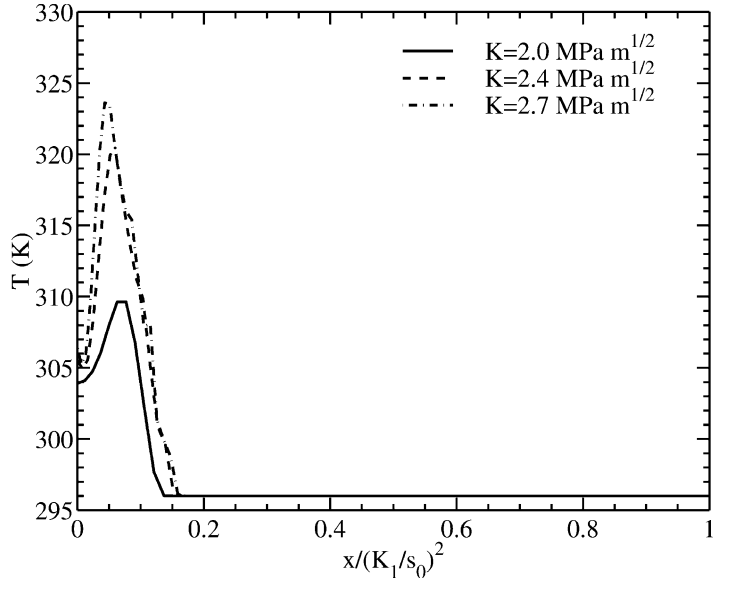

(b)

Fig. 10. Variation of temperature with normalized distance $x/(K_I/s_0)^2$ ahead of the tip for loading rates of (a) 10^2 and (b) 10^6 MPa$\sqrt{\text{m}}$/s, at different values of K_I.

by Sternstein and Myers (1973), Estevez et al. (2000) adopt the criterion that under mode I conditions, a craze initiates when the opening stress σ_{22} attains the condition

$$\sigma_{22} \geqslant \sigma_{\mathrm{m}} - \frac{A^0}{2} + \frac{B^0}{6\sigma_{\mathrm{m}}}. \tag{38}$$

Here, σ_{m} is the hydrostatic stress $(-p)$, and A^0 and B^0 are material parameters, which we chose as 0.68 s_0 and 2.8 s_0^2, respectively (Estevez et al., 2000).

The value K_{crit} of K_{I} at which the criterion given by (38) is satisfied for different loading rates is plotted in Fig. 12 with a solid line. The dashed line in Fig. 12 represents the normalized position $r_{\mathrm{crit}}/(K_{\mathrm{crit}}/s_0)^2$at which the craze is expected to initiate. It is seen that the critical stress intensity factor K_{crit} decreases slightly between 1 and 10^2 MPa$\sqrt{\mathrm{m}}$/s and increases steadily thereafter. Moreover, the point at which craze initiation occurs moves closer to the crack tip with increasing loading rate. It is also evident from Fig. 12 that in the range of loading rates examined in this work, the point of craze initiation lies considerably outside the plastic zone, the size of which is of the order of $\sim (K_{\mathrm{crit}}/s_0)^2$.

The variation of K_{crit} and r_{crit} with loading rate is tied to the distribution of the mean stress σ_{m} ahead of the notch tip. Variation of σ_{m}/s_0 with normalized distance $x/(K_{\mathrm{I}}/s_0)^2$, for different loading rates is shown in Fig. 13 corresponding to a load of $K_{\mathrm{I}} = 1.6$ MPa$\sqrt{\mathrm{m}}$ (which is close to a typical value of K_{crit}). The level of maximum

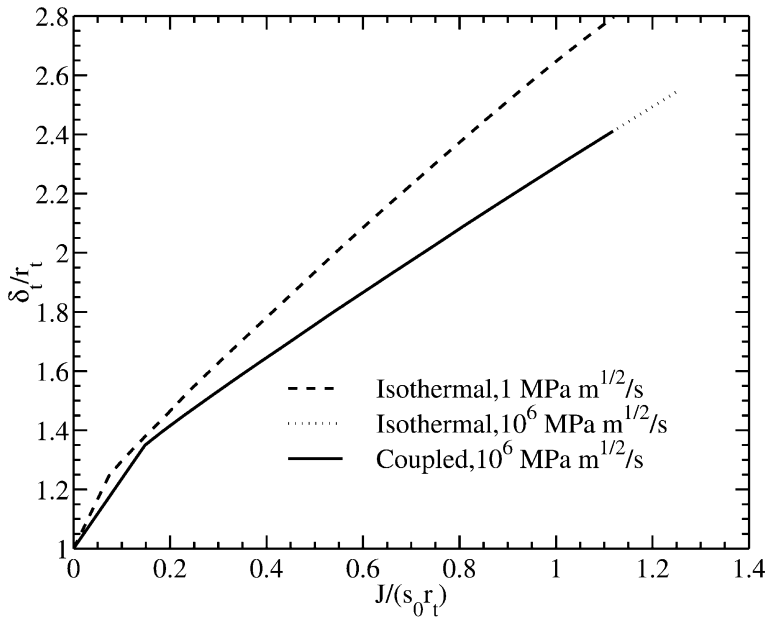

Fig. 11. Variation of the crack tip opening displacement with load $J/(s_0 r_t)$ for different loading rates.

mean stress attained decreases slightly as the loading rate is increased from 1 to 10^2 MPa$\sqrt{\text{m}}$/s. It should be noted at this point that the expression on the right hand side of (38) is a monotonically increasing function of σ_m/s_0 for $\sigma_m/s_0 > 0.7$ [This is incidentally true of all sets of parameters used by Estevez et al. (2000).] This implies that crazing becomes more difficult as the mean stress ahead of the notch tip increases and vice versa. Hence, the value of the critical stress intensity factor, K_{crit}, decreases slightly with decrease in the mean stress. The slight decrease in fracture toughness at moderate loading rates has also been noted by Priest (1976) in connection with some varieties of steel and has been attributed to the effects of thermal conductivity. It should be noted that, in the present work, the effect of thermal conductivity is noticeable around a loading rate of 10^2 MPa$\sqrt{\text{m}}$/s according to (35) (see also, Figs. 4 and 6).

As the loading rate is further increased to 10^4 MPa$\sqrt{\text{m}}$/s, the peak value of the mean stress increases substantially which makes craze initiation more difficult to occur, hence causing the value of K_{crit} to rise. Moreover, the position at which the peak mean stress is attained, and consequently the position at which the condition (38) is satisfied, moves closer to the crack tip with increase in loading rate. It must however be mentioned that it is generally not justified to equate K_{crit} with the fracture initiation toughness of the material. Once a craze is initiated, (unlike a brittle crack which grows catastrophically once it initiates) considerably more energy is needed in order to widen the craze and finally cause breakdown (Estevez et al., 2000).

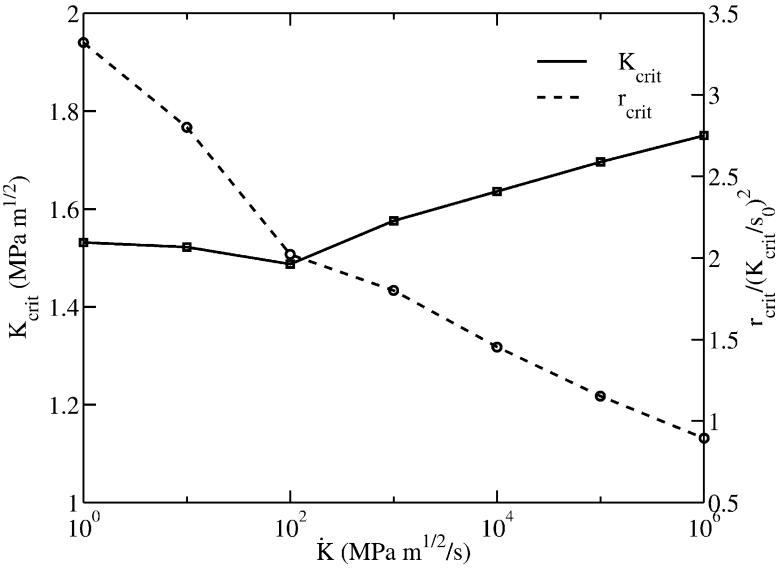

Fig. 12. Variation with loading rate of the critical value of K_I at craze initiation and the normalized distance of the point at which crazing initiates.

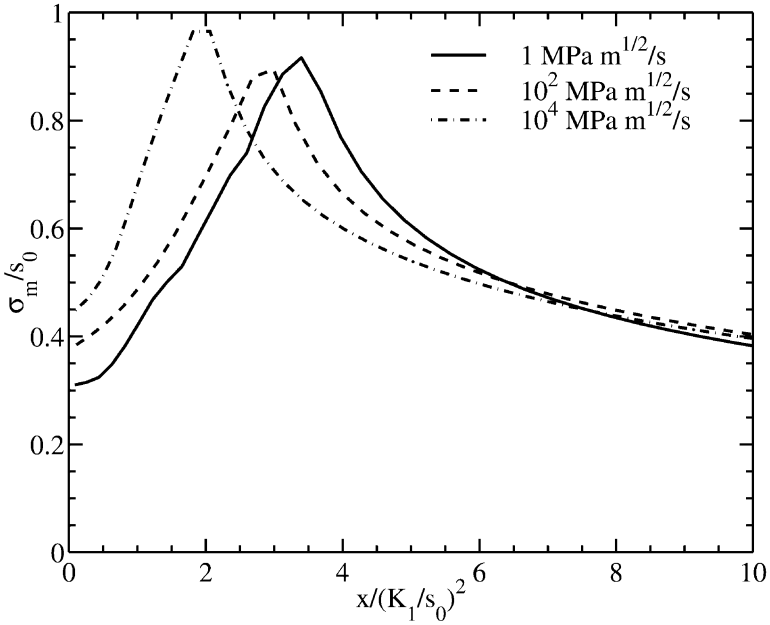

Fig. 13. Variation of the mean stress σ_m with normalised distance ahead of the crack tip at a load level $K_I = 1.6$ MPa$\sqrt{m}$/s for different loading rates.

5. Conclusions

In this paper the thermo-mechanics of finite deformation near cracks in glassy polymers is discussed. A finite element procedure is used to solve the coupled momentum and energy balance equations. This formulation is used to analyze a small scale yielding problem for glassy polymers. Although crack growth by crazing is not considered here, it should be mentioned that, the present model interfaces well with models of crazing based on the 'cohesive zone' methodology (see, Tijssens et al., 2000). A more complete model incorporating the possibility of crack growth by 'crazing' will be the topic of a forthcoming paper.

The salient conclusions from the present analyses are the following:

1. Effects of heat conduction in the material (SAN, in this case) should be taken into account in the loading rate regime between 10^2–10^4 MPa$\sqrt{m}$/s. Isothermal calculations suffice below this range while adiabatic analyses are adequate above it.
2. The major effects of heat diffusion away from the plastic zone are the widening of shear bands, reduced local temperature rise (with respect to load or K_I) and more diffuse heat-affected zones.
3. The stress intensity factor K_{crit} at which craze initiation criterion is satisfied ahead of the crack tip remains almost constant at low rates of loading but

increases steadily thereafter. Also, the point of craze inception moves closer to the crack tip with increase in loading rate.

4. The fracture initiation toughness K_{crit} is reasonable for low values of $\dot{K}$, but underestimates the increase at higher $\dot{K}$.

This points to the fact that the limitations of the analysis, such as $T \leqslant T_g$, stretch independent crazing criterion etc., are probably important in determining the fracture toughness. Further work to investigate these effects should be done and is in progress.

References

Argon, A.S., 1973. A theory for low temperature plastic deformation of glassy polymers. Phil. Mag. 28, 839–865.

Arruda, E.M., Boyce, M.C., Jayachandran, R., 1993. Effects of strain rate, temperature and thermomechanical coupling on the finite strain deformation of glassy polymers. Mech. Mater. 19, 193–212.

Arruda, E.M., Boyce, M.C., Quintus-Bosz, H., 1995. Effects of initial anisotropy on the finite strain deformation behaviour of glassy polymers. Int. J. Plasticity 9, 783–811.

Besseling, J.F., Van der Giessen, E., 1994. Mathematical Modelling of Inelastic Deformation. Chapman & Hall.

Boyce, M., Parks, D.M., Argon, A.S., 1988. Large inelastic deformation of glassy polymers. Part 1: rate dependent constitutive model. Mech. Mater. 7, 15–33.

Buckley, C.P., Jones, D.C., 1995. Glass-rubber constitutive model for amorphous polymers near the glass transition. Polymer. 36, 3301–3312.

Dickinson, J.T., Jensen, L.C., Langford, S.C., Dion, R.P., 1994. Temperature measurements of the gaseous emission during the fracture of polystyrene: a determination of the fracture energy and fracture surface temperature. J. Polymer Sc.: Part B: Polymer Phys 32, 779–784.

Döll, W., 1976. Application of an energy balance and an energy method to dynamic crack propagation. Int. J. Fracture 12, 595–605.

Estevez, R., Tijssens, M.G.A., Van der Giessen, E., 2000. Modeling of the competition between shear yielding and crazing in glassy polymers. J. Mech. Phys. Solids 48, 2585–2617.

Fuller, K.N.G., Fox, P.G., Field, J.E., 1975. The temperature rise at the tip of fast-moving cracks in glassy polymers. Proc. Roy. Soc. Lond. A341, 537–557.

Godovsky, Y.K., 1992. Thermophysical Properties of Polymers. Springer-Verlag, Berlin.

Haward, R.N., Thackray, G., 1968. The use of a mathematical model to describe isothermal stress-strain curves in glassy thermoplastics. Proc. R. Soc. Lond. A302, 453–472.

Lai, J., Van der Giessen, E., 1997. A numerical study of crack-tip plasticity in glassy polymers. Mech. Mater. 25, 183–197.

Pierce, D., Shih, C.F., Needleman, A., 1984. A tangent modulus method for rate dependent solids. Comput. Struct. 18, 875–887.

Priest, A.H., 1976. Influence of Strain Rate and Temperature on the Fracture and Tensile Properties of Several Metallic Materials. Welding Institute-ASM International Conference, Cambridge, UK.

Raha, S., Bowden, P.B., 1972. Birefringence of plastically deformed poly(methyl methacrylate). Polymer 13, 174–183.

Rittel, D., 2000. Experimental investigation of transient thermoplastic effects in dynamic fracture. Int. J. Solids Struct. 37, 2901–2913.

Rudnev, S.N., Salamatina, O.B., Voenniy, V.V., Oleynik, E.F., 1991. Plastic deformation kinetics for glassy polymers and blends. Colloid Polym. Sci. 269, 460–468.

Shih, C.F., 1981. Relationship between the J-integral and crack opening displacement for stationary and extending cracks. J. Mech. Phys. Solids 29, 305–326.

Steenbrink, A.C., Janik, H., Gaymans, R.J., 1997. Deformation and fracture of styrene-acrylonitrile copolymer-rubber blends. Microscopy studies of deformation zones. J. Mater. Sci. 32, 5505–5511.

Sternstein, S.S., Myers, F.A., 1973. Yielding of glassy polymers in the second quadrant of principal stress space. J. Macromo. Sci.— Phys. B 8, 539–571.

Taylor, G.I., Quinney, H., 1934. The latent heat remaining in a material after cold working. Proc. Roy. Soc. Lond. A143, 307–326.

Tijssens, M.G.A., Van der Giessen, E., Sluys, L.J., 2000. Modelling of crazing using a cohesive surface methodology. Mech. Mater. 32, 19–35.

Tomashevskii, E.E., Egorov, E.A., Savostin, A.Ya., 1975. Thermal effects during fracture of polymers. Int. J. Fracture 11, 817–827.

Treloar, L.R.G., 1975. Physics of Rubber Elasticity, third ed. Oxford University Press.

Van der Giessen, E., 1997. Localized plastic deformations in glassy polymers. Euro Mechanics A/Solids 16, 87–106.

Van der Giessen, E., Lai, J., 1999. Temperature effects on crack tip plasticity polymers. In: Bruhns, O.T., Stein, E. (Eds.), IUTAM Symposium on Micro- and Macroscopic Aspects of Thermoplasticity. Kluwer Academic, The Netherlands, pp. 167–176.

Van der Giessen, E., Neale, K.W., 1993. Analysis of the inverse swift effect using a rate-sensitive polycrystal model. Comp. Meth. Appl. Mech. Eng. 103, 291–313.

Williams, J.G., 1972. Visco-elastic and thermal effects on crack growth in PMMA. Int. J. Fracture Mech. 8, 393–401.

Williams, J.G., Hodgkinson, J.M., 1981. Crack-blunting mechanisms in impact tests on polymers. Proc. Roy. Soc. Lond. A375, 231–248.

Wu, P.D., Van der Giessen, E., 1993. On improved network models for rubber elasticity and their applications to orientation hardening in glassy polymers. J. Mech. Phys. Solids 41, 427–456.

Wu, P.D., Van der Giessen, E., 1995. On network descriptions of mechanical and optical properties of rubbers. Philosophical Magazine A71, 1191–1206.

Wu, P.D., Van der Giessen, E., 1995. On neck propagation in amorphous glassy polymers under plane strain tension. Int. J. Plasticity 11, 211–235.

Wu, P.D., Van der Giessen, E., 1996. Computational aspects of localized deformations in amorphous glassy polymers. Eur. J. Mech., A/Solids 15, 799–823.

Zhou, M., Needleman, A., Clifton, R.J., 1994. Finite element simulations of shear localization in plate impact. J. Mech. Phys. Solids 42, 423–458.